EFFECTS OF TURBULENCE MIXING, VARIABLE PROPERTIES, AND VAPORIZATION ON SPRAY DROPLET COMBUSTION

Y.M. Kim and T.J. Chung

Department of Mechanical Engineering
The University of Alabama in Huntsville
Huntsville, Alabama, USA

Point of Contact

Professor T.J. Chung
Department of Mechanical Engineering
The University of Alabama in Huntsville
Huntsville, AL 35899

Telephone: (205) 895–6394

EFFECTS OF TURBULENCE MIXING, VARIABLE PROPERTIES, AND VAPORIZATION ON SPRAY DROPLET COMBUSTION

Y.M. Kim* and T.J. Chung*

ABSTRACT

Combustion of liquid fuels in the form of spray droplets is simulated numerically in this paper. Various vaporization models are examined as to their performance in finite element calculations involving turbulent flow field. The Eulerian Coordinate for the gas and Lagrangian Coordinate for the liquid spray droplets are coupled through source terms being updated in the equations of continuity, momentum, and energy. The k—ϵ and modified eddy breakup models are used for simulating turbulent spray combustion flow field. Numerical results for the droplet trajectories, droplet heating, recirculation characteristics, and effects of evapolation models are evaluated. It is also shown that the finite element method is advantageous in dealing with complex geometries, complex boundary conditions, adaptive unstructured grids.

1. INTRODUCTION

One of the most critical aspects in spray combustion is an adequate vaporization model in which the effect of neighboring droplets on the rates of heat and mass transport and vaporization for any given droplet can be properly taken into account [1,2]. This is particularly important if the ambient gas temperature is high so that droplet life times and droplet heating times are of the same order of magnitude. Difficulties arise also in turbulent flow where the k—ϵ model found satisfactory in nonreacting gas media may not be applicable in reacting spray combustion. A similar question is raised as to the adequacy of modified eddy breakup model to determine the mixing rates of reactants. The main issue in this paper, however, is not the development of such models, but rather the implementation of computational techniques for the turbulent spray combustion using the currently available physical models. Three vaporization models [2,3] are examined.

We present finite element calculations [5] of turbulent spray combustion [6] using the Eulerian Coordinate for the gas and Lagrangian Coordinate for the liquid spray droplets, the k—ϵ turbulence model, the eddy breakup model for predicting the mixing rates of the reactants. In turbulent reacting flows in the Eulerian coordinates, the velocity and pressure fields are strongly coupled with various source terms including turbulence, gas/liquid—phase interaction, and chemical reaction rates.

---

* Research Associate
** Professor

To prevent the spurious pressure modes, the mixed interpolation finite element method is used. Such a coupled solution eliminates the need for transformation of the continuity equation into a pressure or pressure correction equation in the sequential method. The coupled method used here is relatively insensitive to Reynolds numbers and grid aspect ratio. Other transport equations are solved sequentially. The solution procedure for gas–phase equations is similar to the single–phase turbulent reacting flows. The ordinary differential equations governing the droplet field in the Lagrangian coordinates are integrated using an explicit second–order Runge–Kutta method. The gas–phase properties at the characteristic location are calculated by linear interpolation of the four isoparametric finite element Eulerian nodal values in the computational element containing the droplet. The characteristic source terms at the Eulerian grid is evaluated by superimposing the nonlinear source term of each characteristic to the four surrounding grid points using the volume–weighted linear interpolation.

Applications include calculations of droplet trajectories as well as the complete flow field variables in a centerbody combustor. It is shown that the present finite element model predicts the qualitative features of the turbulent spray combustion satisfactorily, pending verification by experimental measurements. The computational results show that the variations of thermophysical properties and the droplet heating model have the significant effects on the droplet history and the gas–phase flowfield near the injection region.

2. GAS FIELD EQUATIONS IN EULERIAN COORDINATES

The governing equations in Eulerian coordinates include equations of continuity, momentum, mass fractions, turbulent kinetic energy, dissipation, and concentration fluctuations.

Continuity

$$\frac{\partial \rho}{\partial t} + \frac{\partial}{\partial x}(\rho u) + \frac{1}{y}\frac{\partial}{\partial y}(y\rho v) = \frac{1}{Re_c}\ \Sigma\ \frac{1}{L_k}\, n_k\, \dot{m}_k \tag{1}$$

with n_k = no. of droplets, and m_k = droplet vaporization rate. Here all variables are time–averaged mean quantities.

Axial Momentum

$$\frac{\partial \rho u}{\partial t} + \frac{\partial}{\partial x}\left[\rho u^2 - \mu_e \frac{\partial u}{\partial x}\right] + \frac{1}{y}\frac{\partial}{\partial y}\left[y\rho uv - y\mu_e \frac{\partial u}{\partial y}\right] = -\frac{\partial p}{\partial x} + \frac{\partial}{\partial x}\left(\mu_e \frac{\partial u}{\partial x}\right) + \frac{1}{y}\frac{\partial}{\partial y}\left(y\mu_e \frac{\partial u}{\partial x}\right)$$

$$+ \frac{1}{Re_c}\Sigma \frac{1}{L_k}\left(n_k \dot{m}_k u_k - \frac{4\pi}{3}\rho_k r_k^3 n_k \frac{du_k}{dt}\right) \tag{2}$$

Radial Momentum

$$\frac{\partial \rho v}{\partial t} + \frac{\partial}{\partial x}\left[\rho uv - \mu_e \frac{\partial v}{\partial y}\right] + \frac{1}{y}\frac{\partial}{\partial y}\left[y\rho v^2 - y\mu_e \frac{\partial v}{\partial y}\right] = -\frac{\partial p}{\partial y} + \frac{\partial}{\partial x}\left(\mu_e \frac{\partial u}{\partial y}\right) + \frac{1}{y}\frac{\partial}{\partial y}\left(y\mu_e \frac{\partial v}{\partial y}\right)$$

$$- \frac{2\mu_e v}{y^2} + \frac{1}{Re_c}\Sigma \frac{1}{L_k}\left(n_k \dot{m}_k v_k - \frac{4\pi}{3}\rho_k r_k^3 n_k \frac{dv_k}{dt}\right) \tag{3}$$

Mass Fraction of Fuel

$$\frac{\partial \rho Y_f}{\partial t} + \frac{\partial}{\partial x}\left[\rho u Y_f - \Gamma_e \frac{\partial Y_f}{\partial x}\right] + \frac{1}{y}\frac{\partial}{\partial y}\left[y\rho v Y_f - y\Gamma_e \frac{\partial Y_f}{\partial y}\right] = -w_f R_{fu} + \frac{1}{Re_c}\Sigma \frac{1}{L_k} n_k \dot{m}_k \tag{4}$$

Mass Fraction of Oxidizer

$$\frac{\partial \rho Y_o}{\partial t} + \frac{\partial}{\partial x}\left[\rho u Y_o - \Gamma_e \frac{\partial Y_o}{\partial x}\right] + \frac{1}{y}\frac{\partial}{\partial y}\left[y\rho v Y_o - y\Gamma_e \frac{\partial Y_o}{\partial y}\right] = -\nu w_o R_{fu} \tag{5}$$

Energy

$$\frac{\partial \rho h}{\partial t} + \frac{\partial}{\partial x}\left[\rho uh - \Gamma_e \frac{\partial h}{\partial x}\right] + \frac{1}{y}\frac{\partial}{\partial y}\left[y\rho vh - y\Gamma_e \frac{\partial h}{\partial y}\right] = \left(-\nu_c - 1\right) M_c^2 \frac{\partial p}{\partial t} + w_f Q R_{fu} + \rho T \frac{Dc_p}{Dt}$$

$$- \frac{\partial}{\partial x}\left(\Gamma_e T \frac{\partial c_p}{\partial x}\right) - \frac{1}{y}\frac{\partial}{\partial y}\left(y\Gamma_e T \frac{\partial c_p}{\partial y}\right) + \frac{1}{Re_c}\Sigma \frac{1}{L_k} n_k \dot{m}_k \left(h_s - \ell_{k,e}\right) \tag{6}$$

Turbulent Kinetic Energy

$$\frac{\partial \rho k}{\partial t} + \frac{\partial}{\partial x}\left[\rho uk - \Gamma_e \frac{\partial k}{\partial x}\right] + \frac{1}{y}\frac{\partial}{\partial y}\left[y\rho vk - y\Gamma_e \frac{\partial k}{\partial y}\right] = \mu_t G - \rho\epsilon \tag{7}$$

Turbulent Energy Dissipation

$$\frac{\partial \rho \epsilon}{\partial t} + \frac{\partial}{\partial x}\left[\rho u\epsilon - \Gamma_e \frac{\partial \epsilon}{\partial x}\right] + \frac{1}{y}\frac{\partial}{\partial y}\left[y\rho v\epsilon - y\Gamma_e \frac{\partial \epsilon}{\partial y}\right] = C_1 C_\mu Gk\rho - C_2 \rho \epsilon^2/k \tag{8}$$

Concentration Fluctuation

$$\frac{\partial \rho g}{\partial t} + \frac{\partial}{\partial x}\left[\rho u g - \Gamma_e \frac{\partial g}{\partial x}\right] + \frac{1}{y}\frac{\partial}{\partial y}\left[y\rho v g - y\Gamma_e \frac{\partial g}{\partial y}\right] = C_{g_1}\mu_e\left[\left(\frac{\partial Y_f}{\partial x}\right)^2 + \left(\frac{\partial Y_f}{\partial y}\right)^2\right] - C_{g_2}\rho g \frac{\epsilon}{k} \tag{9}$$

where

$$L_k = \frac{r'_c}{r'_{k,o}}, \qquad \mu_e = \frac{\mu_\ell}{Re_c} + \mu_t, \qquad \Gamma_e = \frac{\mu_\ell}{\sigma_{\phi\ell} Re_c} + \frac{\mu_t}{\sigma_{\phi t}}, \qquad \mu_t = c_\mu \rho \frac{k^2}{\epsilon}$$

$$G = 2\left[\left(\frac{\partial u}{\partial x}\right)^2 + \left(\frac{\partial v}{\partial x}\right)^2 + \left(\frac{v}{y}\right)^2\right] + \left(\frac{\partial y}{\partial y} + \frac{\partial v}{\partial x}\right)^2,$$

with σ_ϕ representing Schmidt or Prandtl number for the dependent variable ϕ. Note also that the gas–phase equations are non–dimensionalized using the inflow conditions of the combustor under study, leading to Re_c, the characteristic Reynolds number, M_c, the characteristic Mach number, and L_k, the ratio of the gas–phase length scale to the initial droplet radius of the k th group.

The reaction rate R_{fu} is determined from either the mixing rates of the reactants or the chemical reaction, whichever slower. The mixing rates of the reactants are obtained by the eddy breakup reaction model [7] assuming that the gas is composed of alternating fragments of unburned fuel and almost fully burned gas. The eddy breakup reaction rate is assumed to depend on the rate $\sqrt{g}$ at which the fragments of unburned fuel are broken into smaller fragments by the action of turbulence, and is taken to be proportional to the decay of turbulence energy ϵ/k.

The reaction rate may also be controlled by chemical kinetics when the mixing to the reactants is rapid [8]. Thus the reaction rate is expressed as

$$R_{fu} = \min \begin{cases} A \left(\frac{\rho Y_f}{W_f}\right)^a \left(\frac{\rho Y_o}{W_o}\right)^b \exp\left(-\frac{E}{RT}\right) \\ \frac{C_R}{W_f} \sqrt{g}\left(\frac{\rho \epsilon}{k}\right) \end{cases} \tag{10}$$

The specific heat of the mixture is given by

$$C_p = \sum_i Y_i C_{p,i}(T) \tag{11}$$

Here by assuming equal binary diffusion coefficients for all the species and by knowing the mass fractions of fuel and oxidizer and the stoichiometric relationship of the given hydrocarbon—air mixture, the mass fractions of the remaining species (O_2, N_2, CO_2, and H_2O) can be determined. The variation of the specific heat, with temperature may be written as [9, 10].

$$C_{p,i} = \frac{R}{W_i}\left(C_{1i} + C_{2i}T + C_{3i}T^2 + C_{4i}T^3\, C_{5i}T^4\right)$$

The density distribution in the gas phase is calculated from

$$\rho = P \Big/ RT\, \Sigma\, Y_i/W_i \tag{12}$$

The model constants used in the above equations are as follows: $C_1 = 1.44$, $C_2 = 1.92$, $\mu = 0.09$, $\sigma_k = 1.0$, $\sigma_\epsilon = 1.217$, $\sigma_y = 0.9$, $\sigma_g = 0.9$, $\sigma_h = 0.9$, $C_{g2} = 2.8$, $C_{g2} = 2.0$.

3. LIQUID SPRAY DROPLET FIELD EQUATIONS IN LAGRANGIAN COORDINATES

The liquid—phase equations are based on the Lagrangian formulation of the droplet trajectory, transient heating, and vaporization. The effective conductivity model used in the present study assumes the quasi—steadiness in the gas film. The instantaneous vaporization rate of the droplet is controlled by the transient process of heating of the liquid inside the droplet. In the limiting cases of the droplet impingement on the chamber walls the droplets undergo instantaneous vaporization. The governing equations for the liquid—phase are as follows:

Velocities

$$\frac{dx_k}{dt} = u_k\,, \qquad \frac{dy_k}{dt} = v_k \tag{13}$$

Rate of Change of Velocities

$$\frac{du_k}{dt} = \left(\frac{L_k^2}{Re_c \rho k}\right)\frac{3}{16}\,\frac{C_D \mu Re_k}{r_k^2}\left(u_g - u_k\right) \tag{14}$$

$$\frac{dv_k}{dt} = \left(\frac{L_k^2}{Re_c \rho k}\right)\frac{3}{16}\,\frac{C_D \mu Re_k}{r_k^2}\left(v_g - v_k\right) \tag{15}$$

Reynolds Number

$$Re_k = 2\left(\frac{Re_c}{L_k}\right)\frac{r_k \rho_g}{\mu}\left[\left(u_g - u_k\right)^2 + \left(v_g - v_k\right)^2\right]^{\frac{1}{2}} \tag{16}$$

Drag Coefficient

$$C_D = \frac{24}{Re_k}\left(1 + \frac{Re_k^{\frac{2}{3}}}{6}\right) \tag{17}$$

Various evaporation models have been proposed and they appear to be quite sensitive in numerical applications. The droplet evaporation rate and the heat balance equation may be expressed as

$$\frac{dr_k}{dt} = -\dot{m}_k \Big/ 4\pi \rho_k r_k^2 \tag{18}$$

$$\dot{m}_k = N_A N_B \tag{19}$$

and

$$\frac{dT_k}{dt} = \frac{Q_L}{m_k C_{pk}} \tag{20}$$

where $\dot{m}_k$ is the evaporation rate; N_A and N_B denote the evaporation coefficient and the correction factor for convection effects, respectively; T_k is the droplet surface temperature; Q_L is the heat transferred into the droplet interior; m_k is the droplet mass; C_{pk} is the specific heat of the droplet. We consider the following two models:

(a) **Model I** [3]

In this model the evaporation coefficient and the correction factor for convection effects are given by

$$N_A = 4\pi r_k \lambda g \Big/ C_{pg}\, \ell n\left(1 + B_M\right), \qquad N_B = 1 + 0.276\, Re_k^{\frac{1}{2}}\, Pr^{\frac{1}{3}}$$

where B is the mass transfer number. The heat energy, Q_L, takes the form

$$Q_L = \dot{m}\left(\frac{C_{pg}(T - T_k)}{B_M} - H_v\right)$$

with

$$B_M = \frac{Y_{fs} - Y_{f\infty}}{1 - Y_{fs}} , \qquad Y_{fs} = \left[1 + \left(\frac{P}{P_{fs}} - 1\right)\frac{W_a}{W_f}\right]^{-1}$$

Here Y_{fs} and P_{fs} are the mass fraction and the fuel vapor pressure at the droplet surface, respectively; P, the ambient pressure, is the sum of the fuel vapor pressure and the air partial pressure at the droplet surface; W_a and W_f are the molecular weights of fuel and air, respectively. For any given value of surface temperature, the vapor pressure is readily estimated from modified Clausius—Clapeyron equation.

$$P_{fs} = \exp\left[a_1 - a_2/\left(T_k - a_3\right)\right]$$

Values of a_1, a_2, and a_3 are found in [3,4]. If the heat transfer to the droplet interior is neglected, then we set $H_{v,eff} = H_v$. Also, to keep the heat transfer rate of vaporization ($\dot{m}\, H_{v,eff}$) positive, it is necessary to maintain $Y_{f\infty} = 0$.

(b) **Model II** [3]

Model II is the same as Model I except for the effective latent heat of vaporization. Considering the heat transferred in the droplet interior (Q_L), the effective latent heat of vaporization can be obtained from

$$H_{v,eff} = H_v + Q_L/\dot{m} = \frac{B_t}{B_m} H_v$$

with

$$B_t = \frac{C_{pg}\ (T - T_k)}{H_v}$$

where B_t is the heat transfer number

(c) **Model III** [4]

This model includes the effects of variable thermophysical properties, non—unitary Lewis number in the gas film, the effect of the Stefan flow on heat and mass transfer between the droplet and the gas, and the effect of internal circulation and transient liquid heating. Thus, the evaporation coefficient and the correction factor for convection effects are as follows:

$$N_A = 4\pi r_k \rho_g D_g \ln\left(1 + B_M\right) , \qquad N_B = 1 + \left(Sh_0/2 - 1\right)/F\left(B_M\right)$$

with

$$F(B) = (1+B)^{0.7} \frac{\ln(1+B)}{B} \qquad \text{(film thickness correction)} \tag{21}$$

$$Sh_0 = 1 + \left(1 + Re_k\, Sc\right)^{\frac{1}{3}} f\left(Re_k\right) \tag{22}$$

$$f\left(Re_k\right) = \begin{cases} 1 & \text{for } Re_k \leq 1 \\ Re_k^{0.077} & \text{for } 1 \leq Re_k \leq 400 \end{cases} \tag{23}$$

The heat energy takes the form

$$Q_L = \dot{m} \left[\frac{C_{pf}(T - T_k}{B_T} - H_v\right]$$

where

$$B_T = \left(1 + B_M\right)^{\phi} - 1 \ , \qquad \phi = \frac{C_{pf}}{C_{pg}} \frac{Sh^*}{Nu^*} \frac{1}{L_e}$$

$$L_e = \lambda_g \Big/ \rho_g\, D_g\, C_{pg} \ , \qquad Sh^* = C_b$$

$$Nu^* = 1 + \left(Nu_0/2 - 1\right)\Big/ F\left(B_T\right) \ , \qquad Nu_0 = 1 + \left(1 + Re_k\, Pr\right)^{\frac{1}{3}} f\left(Re_k\right)$$

The average properties of air—vapor mixture may be determined at the following reference temperatures and compositions [11]:

$$T_{ref} = T_k + \frac{1}{3}\left(T - T_k\right) \ , \qquad Y_{fr} = Y_{fs} + \frac{1}{3}\left(Y_{fs} - Y_{f\infty}\right)$$

In the limiting cases of the droplet impingement on the chamber walls, the droplets undergo instantaneous vaporization. A similar treatment of the droplet is considered when approximately 97% of the mass of the droplets is vaporized. In case of the droplet passage through the plane of symmetry, another droplet with similar instantaneous properties and physical dimensions, but with the mirror image velocity vector is injected into the flow field.

4. COUPLING OF LIQUID AND GAS PHASES

The liquid—phase equations for spray droplets are advanced in time by an explicit second— order Runge—Katta method using time steps much smaller than the gas—phase equations. Based on the known

gas—phase properties, the liquid—phase equations are first advanced in time from the nth time level to the (n+1)th time level corresponding to the gas—phase time step Δt_g as follows:

(1) Interpolate linearly the gas—phase properties from the fixed Eulerian locations to the characteristic location.

(2) Integrate the liquid—phase equations over a time step, Δt_ℓ.

(3) Redistribute the source terms evaluated at the characteristic location among the Eulerian nodes surrounding the characteristic.

(4) Steps (1) — (3) are repeated until the liquid—phase equations are advanced over a time step, Δt_g.

(5) Solve the gas—phase equations using the time implicit scheme.

(6) Repeat steps (1) — (5) until the iteration converges before advancing to the next step.

The injected spray and the droplet flow is assumed to be conical such that

$$u_k = u_{k,o} \cos\theta \ , \qquad v_k = v_{k,o} \sin\theta$$

where θ is the half—cone angle. The mass flow rate of the fuel is determined from the stoichiometric conditions and the injection time interval for a new characteristic to appear is based on the Eulerian mesh size Δx and injection velocity $u_{k,o}$ of the droplet.

$$dt = \frac{\Delta x}{u_{k,o}}$$

Thus the number of droplets in each characteristic is given by

$$n_k = L_k^3 \frac{M_{f,k} dt}{\frac{4}{3}\pi r_k^3 \rho_k}$$

where $M_{f,k}$ is the mass flow rate is related to

$$M_f = \Sigma \ M_{f,k} = 0.21 \ \phi \ m_a \ W_f / \nu W_o$$

Once the droplets are injected its subsequent behavior is determined by the governing equations.

5. BOUNDARY CONDITIONS

Steep gradients and a relatively low level of turbulence prevail along the wall. To account for rapid changes in velocity profile close to the wall, the so—called wall function method is employed [12]. In the context of finite elements, we assume that the shear stress is constant up to a distance δ from the wall

such that

$$\tau_w = \begin{cases} \mu \dfrac{u}{\delta} & \text{for } \delta^+ < 11.6 \\ \dfrac{\rho \; ku \; C_u^{\frac{1}{4}} \; k^{\frac{1}{2}}}{\ell n E \delta^+} & \text{for } \delta^+ \geq 11.6 \end{cases}$$

with

$$\delta^+ = \frac{\rho \delta \; C_u^{\frac{1}{4}} \; k^{\frac{1}{2}}}{\mu}$$

Once the near—wall values of the shear stresses are evaluated, we calculate the near—wall values of the k and ϵ as follows:

$$k = \frac{|\tau_w/\rho \;|}{C_\mu^{\frac{1}{2}}}, \qquad \epsilon = \frac{|\tau_w/\rho \;|^{3/2}}{\kappa \delta}$$

The near—wall heat flux is determined by

$$\dot{q}_w = \begin{cases} \dfrac{\mu \; C_p \; (T - T_w)}{Pr \qquad \delta} & \text{for } \delta^+ < 11.6 \\ Pr_t = \left[\dfrac{1}{\kappa} \; \ell n \left(E\delta^+\right) + \dfrac{P(pr)}{Pr_t}\right] & \text{for } \delta^+ \geq 11.6 \end{cases}$$

where the function P(pr) is of the form.

$$\frac{P \; (Pr)}{Pr_t} = 9.24 \left[\left(\frac{Pr}{Pr_t}\right)^{3/4} - 1\right]\left[1 + 0.28 \exp\left(-0.007 \frac{Pr}{Pr_t}\right)\right]$$

Here τ_w and $\dot{q}_w$ are specified as Neumann boundary conditions in the momentum and energy equations.

6. APPLICATIONS

Numerical results include comparisons of three different models of vaporization models applied to a typical turbulent spray combustion. Figures 1.a through 1.d show the vaporization characteristics of n—decane droplets of initial radius $r_{k,o} = 50$ μm and $T_{k,o} = 300^{\circ}$K which are injected into the air stream at $P_\infty = 10$atm, $T_\infty = 1500^{\circ}$K, and $\Delta u_o = u - U_k = 10$m/s. The temporal variation of the non—dimensional droplet surface area, surface temperature, vaporization rate ($\dot{m}/m_o$), effective heat transfer rate of evaporation ($\dot{m}H_{v,eff}$), are shown in Figures 1.a, 1.b, 1.c, and 1.d, respectively. Here m_o is the initial droplet mass.

The numerical results indicate that the droplet heating process takes a considerable part of the droplet lifetime. Note here that the vaporization histories of Model 1 are the same as those of Model 2 except when the effective vaporization heat transfer rate is used for Model 2. The transient heating period of Model 1 or Model 2 is much shorter than Model 3. At the final stage, the droplet surface temperature for both models approaches an equilibrium value which is the wet—bulb temperature. Model 1 or Model 2 leads to a higher wet—bulb temperature than Model 3. Since the transfer number of Model 3 is based on the effective latent heat vaporization, Model 3 has a slower vaporization than Model 1 or Model 2 in the initial heating period. Figure 1.d shows the temporal variations in the effective heat transfer vaporization ($\dot{m}H_{v,eff}$). Models 2 and 3 have the large heat transfer rate in the early evaporation period which is controlled by the effective latent heat vaporization. However, the heat transfer rate of vaporization for Model 1 is controlled by the vaporization rate because the effective latent heat in Model 1 is obtained by neglecting the heat transfer to the droplet interior. Since Model 2 has a faster vaporization than Model 3 in the droplet heating period, Model 2 shows a larger effective heat transfer rate than Model 3.

Figures 2.a through 2.d show the vaporization characteristics of n—decane droplets in the air—fuel mixture medium with $Y_{f\infty} = 0.4$. All other conditions are the same as the previous example. This situation is frequently encountered in the actual spray combusting flows. The vaporization history of Model 1 is the same as the previous case because this model does not account for the effect of the ambient fuel vapor. The introduction of any cold droplet into a surrounding of its own vapor results in vapor condensation on the droplet surface. In the condensation period, the mass transfer number, B_M, becomes negative if the mass fraction of fuel at the interface is less than the mass fraction of fuel at the ambient. As a result, the droplet undergoes the increase in radius. It can be seen that the droplets with its ambient fuel vapor evaporates much faster than the previous case without the ambient fuel vapor. In fuel vapor environment, the droplet Reynolds number increases due to variable property effects related to the liquid dynamic viscosity. The effect of an increase in Reynolds number on heat and mass transfer obviously causes the Nusselt number and Sherwood number to increase. Therefore, the higher droplet

Reynolds number results in increase of the vaporization rate. During the condensation period, Model 2 yields a larger condensation rate than Model 3. Shortly after the condensation period, Model 2 exhibits a faster vaporization than Model 3. However, at the final stage of vaporization, Model 2 shows a slower evaporation than Model 3. Model 2 yields a larger effective heat transfer rate than Model 3 during the entire vaporization period except for the condensation period and the final stage.

The next example is for the computation of the spray combusting flows using three vaporization models with the geometry of a centerbody combustor shown in Figure 3 and the initial and boundary conditions summarized in Table 1. The dimensions of the combustor are the same as those used in Raju and Sirignano [13]. However, the present study uses the variable thermophysical properties. The injected spray is assumed to comprise four conical streams and half—angles of the corresponding streams at θ = 5, 15, 25, and 35 degrees. The computations are performed for three vaporization models discussed earlier. In the limiting cases of the droplet impingement on the chamber walls, the droplets undergo instantaneous vaporization. Similar treatment of the droplet is considered when 97% of the mass of the droplet is vaporized. In case of the droplet passage through the plane of symmetry, another droplet with similar instantaneous properties and physical dimensions but with the mirror image velocity vector is injected into the flowfield. The time steps for the steady state are:Δt_{inj} = 1.6 m/s, Δt_{g} = 1.6 ms, and $\Delta t_{l,m}$ = 0.04ms.

Figures 4.a through 4.c show droplet trajectories and vaporization processes for three vaporization models. The four droplet groups can be identified by the volume of the droplet and the characteristic location. It is seen that the droplet motion is initially governed by the droplet inertia force before the drag force causes the droplets to decelerate and the droplet path is eventually determined by the gas—phase flow field. Most of the vaporization occurs within the recirculation zone because the smaller droplets are unable to penetrate downstream. Because of the strong negative radial gas—phase velocity field near the injector, the droplet trajectories are significantly affected by the gas—phase velocity field especially for the droplet characteristic with the lowest injection angle, θ = 5 degrees.

The strong negative radial gas–phase velocity field in the injector region results from the large drag force term interacting with the source terms of radial momentum equation. Model 1 has a faster evaporation rate than two other models. Slight differences between Model 2 and Model 3 exist in the droplet trajectories corresponding to the final stage of vaporization.

Velocity vectors for three vaporization models are shown in 5.a through 5.c. The velocity field for three models has the similar secondary recirculation zone. This is due to the gas–droplet interaction in recirculation zone having the high vaporization rate. Slight differences among three models exists in the downstream side of the recirculation region.

Figure 6 shows contours of temperature for three vaporization models. The temperature difference between two adjacent lines is about 150^{o}K. The maximum and minimum temperatures of the gas–field are about 2800^{o}K and 700^{o}K. The low temperature near the injector results from the cooling effect of the vaporization process. This region is also characterized by large temperature gradients.

Radial profiles of temperature for three vaporization models are presented in Figure 7. Since the effective latent heat for Model 1 predicts a much higher temperature than the other two models in the fuel–rich side of three axial locations, Model 1 exhibits the highest temperature, followed by Model 3 and Model 2. Temperature distributions in the fuel–rich region mainly depend on the effective heat transfer rate of vaporization ($\dot{m}\, H_{v,eff}$).

Figure 8 shows contours of the fuel mass fraction for three vaporization models. The values of the contour lines vary from 0.005 to 0.655 with the mass fraction difference of 0.05. The large concentration of fuel vapor in the recirculation region is due to insufficient mixing of fuel and air.

Finally, radial profiles of the fuel mass fraction for three vaporization models are shown in Figure 9. Since Model 1 predicts a faster evaporation due to a higher temperature near the injector region (x = 0.004m), Model 1 yields a much larger fuel mass fraction than the other two models. At some distance from the injector (x = 0.08m,0.12m), Model 1 predicts the lowest mass fuel fraction resulting from the shortest droplet lifetime with the high gas–temperature environment. Model 2 shows a larger fuel mass fraction than Model 3 at some distance downstream (x = 0.08m, 0.12m), because Model 2 yields a faster evaporation related to the complex effects of variable properties.

7. CONCLUSIONS

Numerical analysis using the finite element Eulerian–Lagrangian approach for various vaporization models for turbulent spray combustion has been shown to be effective. The following comments are offered:

(1) Variations of the thermophysical properties and the droplet vaporization models are sensitive to the droplet histories and the gas–phase flowfield especially close to the fuel injector region.

(2) Droplet trajectories are greatly influenced by the choice of existing vaporization models which determine the vaporization rate and the effective latent heat of vaporization.

(3) Model 1 has a faster vaporization rate, leading to the droplet trajectories affected more rapidly by the gas–phase flowfield than Models 2 and 3.

(4) The gas–phase velocity field for all vaporization models appears to have a similar secondary recirculation zone. The gas–droplet interactions play a negligible role for the formation of secondary recirculation zone.

(5) Temperature distributions near the fuel–rich injector are significantly affected by the transient droplet heating in terms of the effective latent heat of vaporization. Model 1 predicts the highest temperature distributions, followed by Model 3 and Model 2.

(6) Close to the fuel injector, Model 1 yields a much larger fuel mass fraction than the other two models, reversing the trend downstream because of the shortest droplet lifetime with the higher gas–phase temperature distribution.

(7) Model 2 predicts a slightly larger fuel mass fraction than Model 3 downstream, due to a faster evaporation rate.

(8) In terms of computational strategies, the finite element method would be convenient in dealing with complex geometries, boundary conditions, and adapative unstructured grids.

REFERENCES

1. Faeth, G.M., "Spray Combustion Models — A Review", AIAA Paper 79—0293, 17th Aerospace Science Meeting, New Orleans, 1979.

2. Sirignano, W.A., "The Formulation of Combustion Models: Resolution Compared to Droplet Spacing", ASME Journal of Heat Transfer, Vol. 108, 1986, pp. 633—639.

3. Chin, J.S., and Lefebvre, A.H.,"The Role of the Heat—up Period in Fuel Drop Evaluation", AIAA Paper 83—0068, 21st Aerospace Sciences Meeting, Reno, Nevada, 1983.

4. Abramzon, B., and Sirignano, W.A., "Droplet Vaporization Model for Spray Combustion Calculations", AIAA Paper 88—0636, 26th Aerospace Sciences Meeting, Reno, Nevada, 1988

5. Chung, T.J., Kim, Y.M., and Sohn, J.L., "Finite Element Analysis in Combustion Phenomena", International Journal of Numerical Methods in Fluids, Vol. 7, pp. 989—1012, 1987.

6. Kim, Y.M., and Chung, T.J., "Turbulent Spray Combustion Using Finite Elements", AIAA Paper 89—2483, 1989.

7. Spalding, D.B., "Mathematical Models of Turbulent Flames: A Review", Combustion Science and Technology, Vol. 13, 1976, pp. 3—25.

8. Westbrook, C.K., and Dryer, F.L., "Chemical Kinetic Modeling of Hydrocarbon Combustion", Progress of Energy and Combustion Science, Vol. 10, 1984, pp 1—57.

9. CRC, Handbook of Physics and Chemistry, Chemical Ruber Co., Cincinnati, Ohio, 1978.

10. McBride, B.J., Heimel, S., Fhleers, J.G., Gordon, S., "Thermodynamic Properties to 6000^{0}K for 210 Substances Involving the First 18 Elements", NASA SP—3001, 1963.

11. Hubbard, G.L., Denny, V.E., and Mills, A.F., "Droplet Vaporization: Effects of Transients and Variable Properties", International Journal of Heat and Mass Transfer, Vol. 18, 1975, pp. 1003—1008.

12. Launder, B.E., and Spalding, D.B., "The Numerical Computations of Turbulent Flows", Computer Methods Applied Mechanical Engineering, Vol. 3, 1974, pp. 269—289.

13. Raju, M.S., and Sirignano, W.A., "Spray Computations in a Centerbody Combustor", Proceedings of the 1987 ASME/JSME Thermal Engineering Joint Conference, Vol. 1.

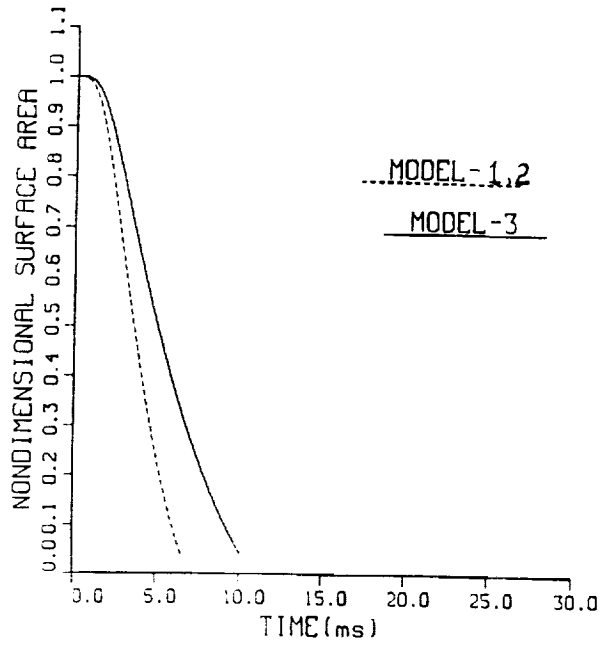

(a) Droplet Surface Area

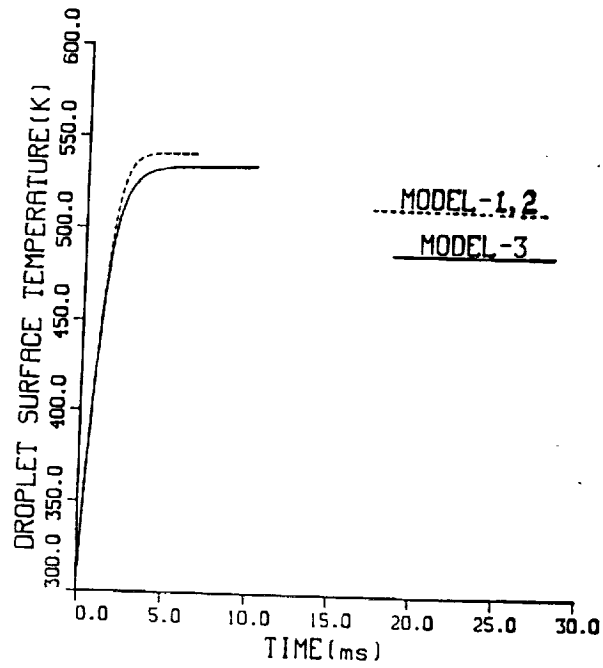

(b) Surface Temperature

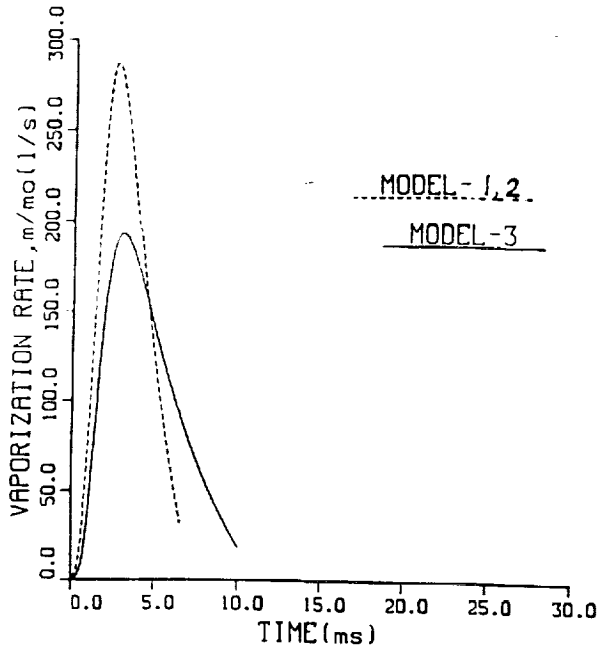

(c) Vaporization Rate

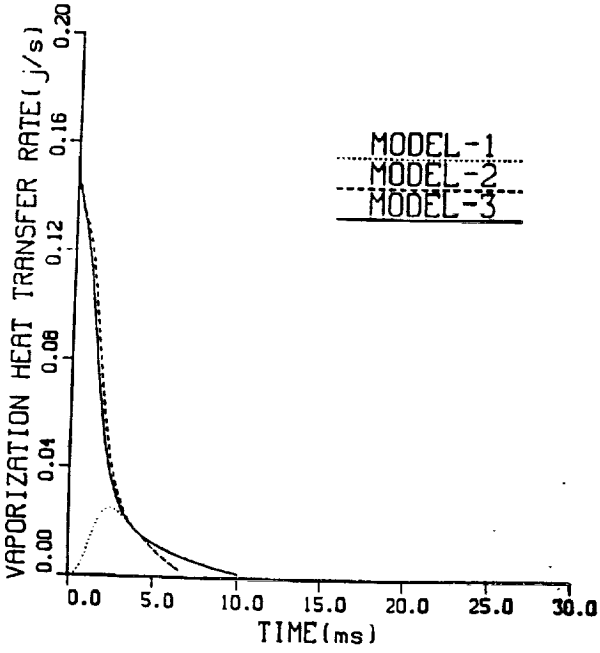

(d) Effective Heat Transfer Rate of Evaporation

Fig 1 Vaporization Characteristics on n–decane droplets injected into air flow.
$r_{k,o} = 50\ \mu m$, $T_{k,o} = 300°K$, $P_\infty = 10$ atm, $T_\infty = 1500°$, $\Delta u_o = u - U_k = 10 m/s$

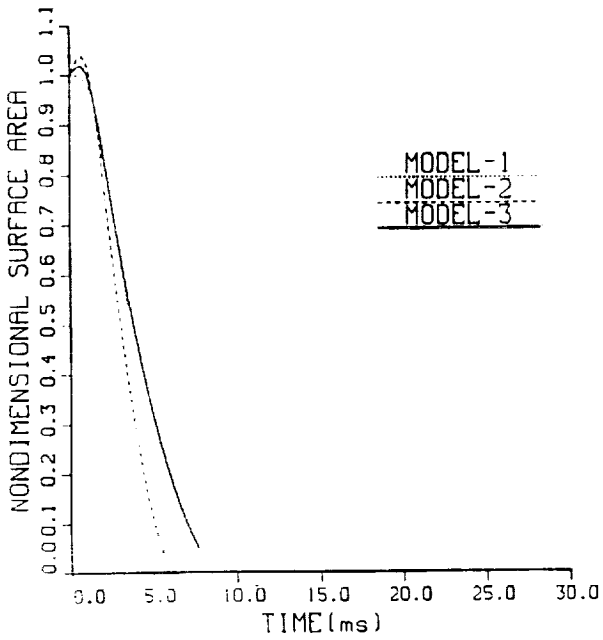

(a) Droplet Surface Area

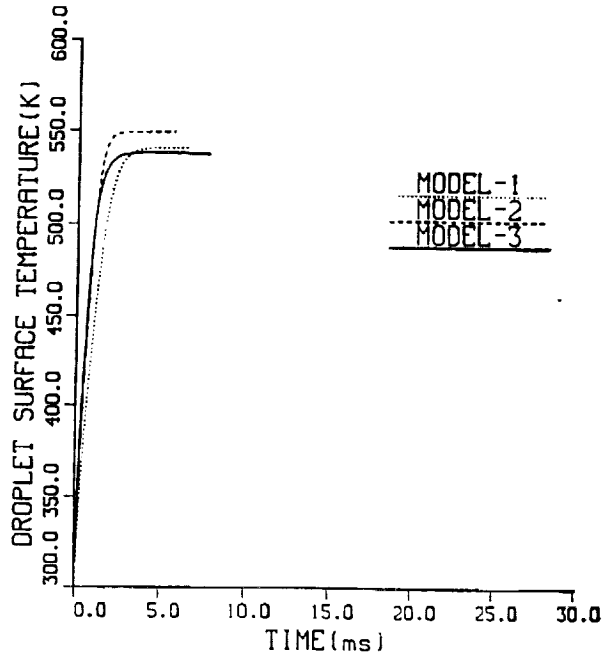

(b) Surface Temperature

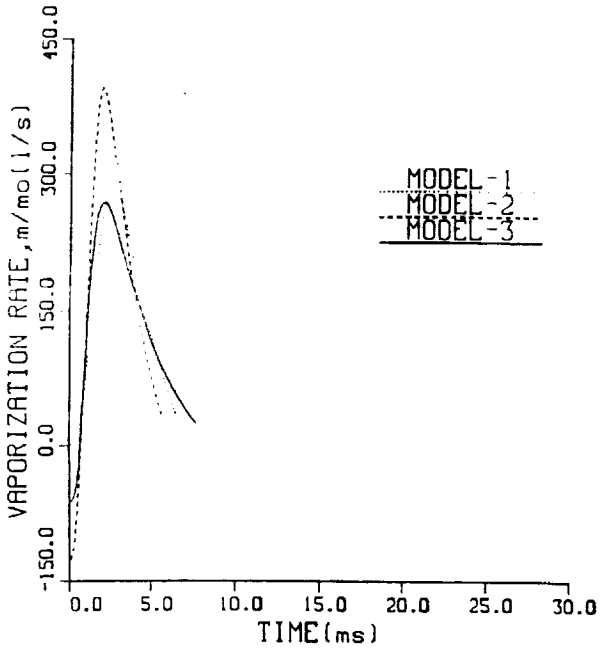

(c) Vaporization Rate

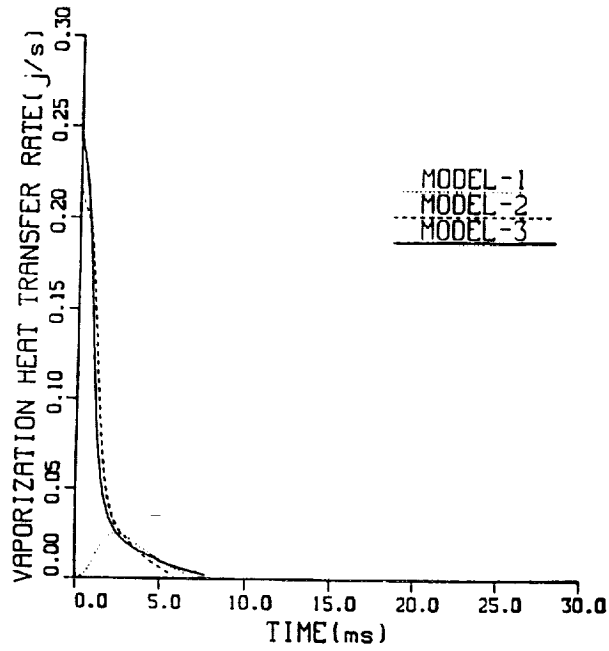

(d) Effective Heat Transfer Rate of Evaporation

FIG 2 Vaporization Characteristics of n–decane droplets in the Air–fuel Mixture Medium with $Y_{f\infty} = 0.4$

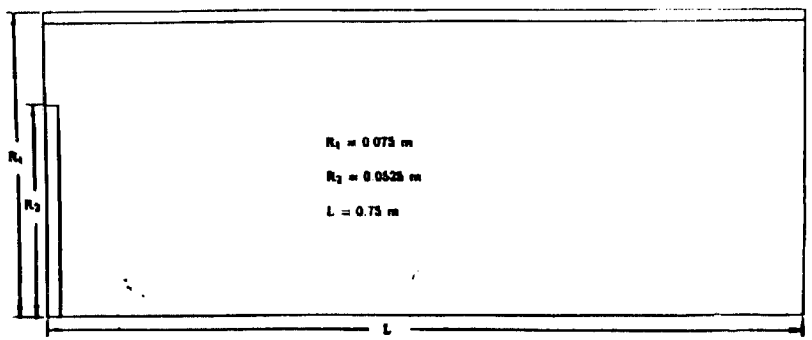

FIG 3 Geometry of Computational Domain, Finite Element Discretization, 29 x 24 with Finer Meshes in the Vicinity of Recirculation Zone, Injector Angles, $\theta = 5^{\circ}, 15^{\circ}, 25^{\circ}, 35^{\circ}$, $\Delta t_{inj} = 1.6$ m/s, $\Delta t_{g} = 1.6$ ms, $\Delta t_{l,m} = 0.04$ ms

Gas—phase boundary conditions		Liquid—phase initial conditions	
Velocity (m/s)	30	Fuel	n—decane
Temperature (K)	1000	Liquid density(kg/m^3)	773
Pressure (atm)	10	Droplet temperature(K)	300
Density (kg/m^3)	3.399	Droplet velocity(m/s)	20
Duct wall temperature(K)	700	Equivalent ratio	0.3
Centerbody wall temperature(K)	1000	Air flow rate(kg/s)	0.9
Tubulent kinetic energy(m^2/s^2)	$0.01u^2_{in}$	Fuel flow rate(kg/s)	0.018

TABLE 1 Gas and Fuel Liquid Properties

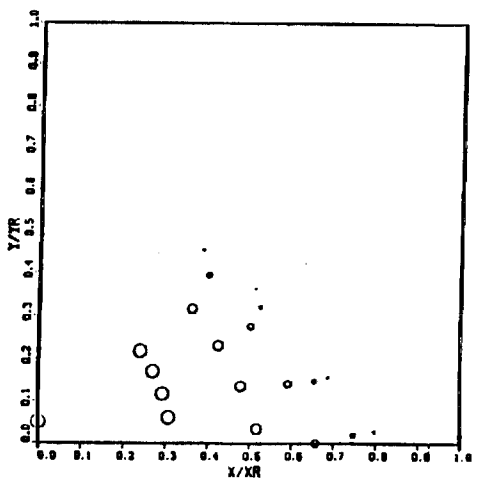

(a) Model I

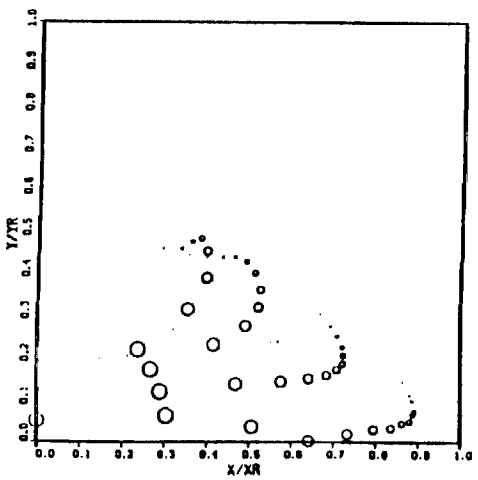

(b) Model II

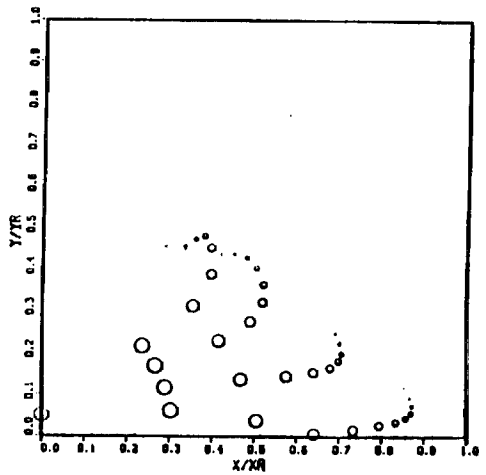

(c) Model III

FIG 4 Droplet Trajectories and Vaporization Process

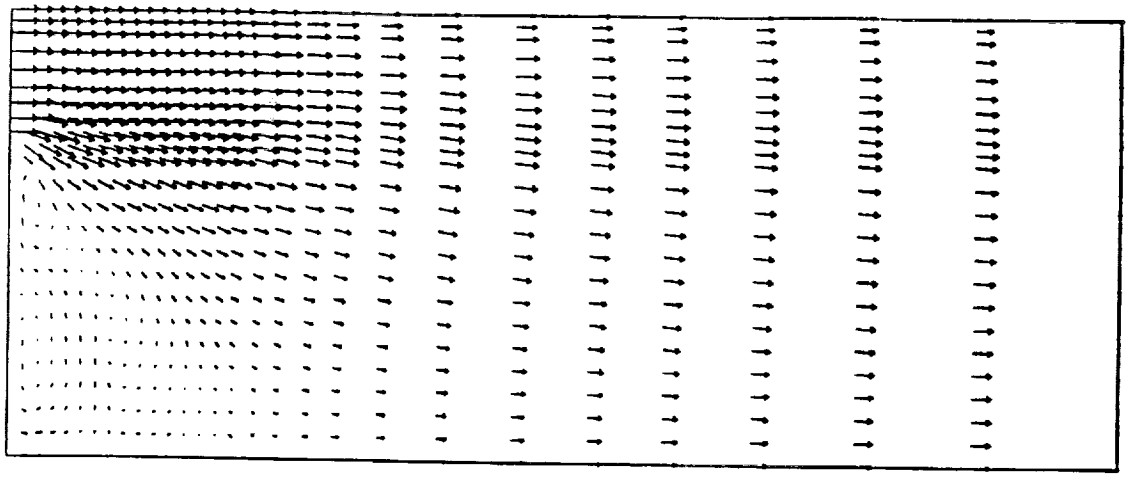

(a) Model I

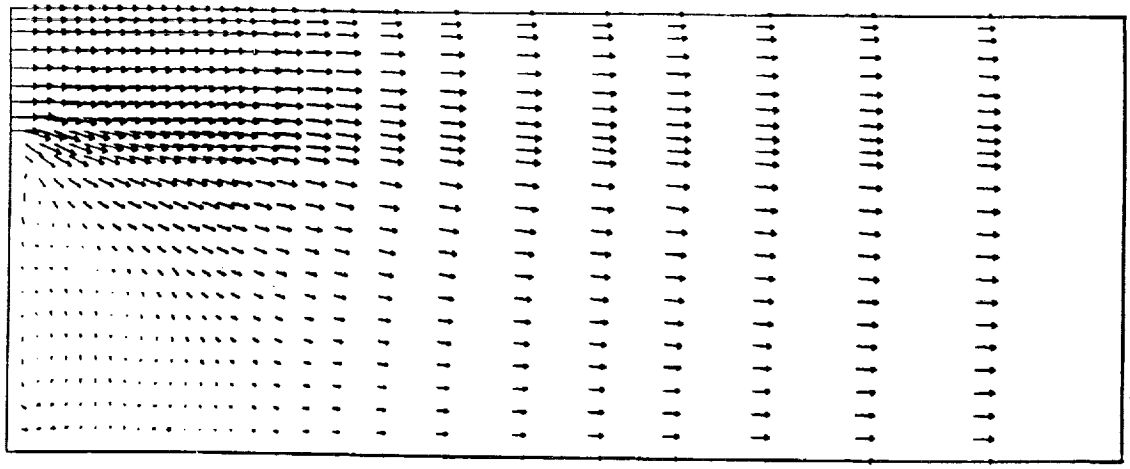

(b) Model II

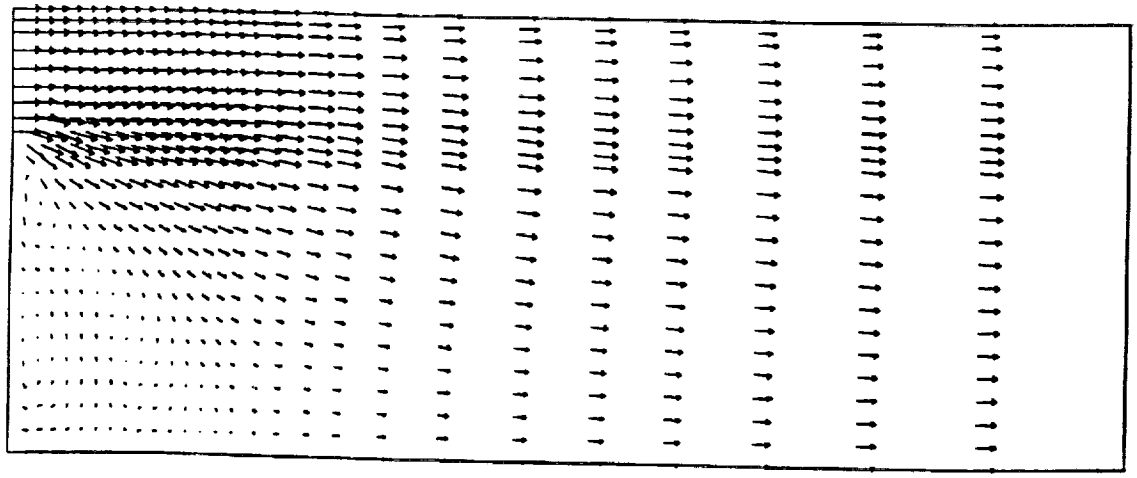

(c) Model III

FIG 5 Velocity Vectors

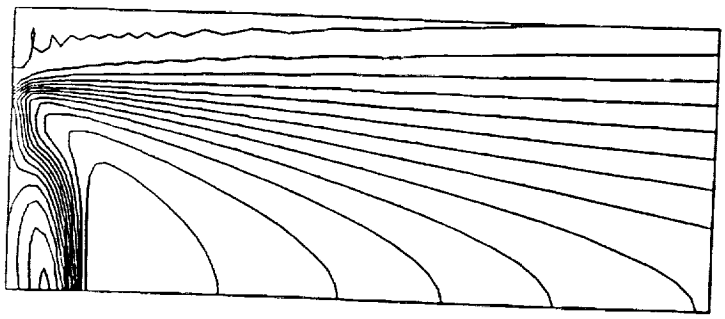

(a) Model I

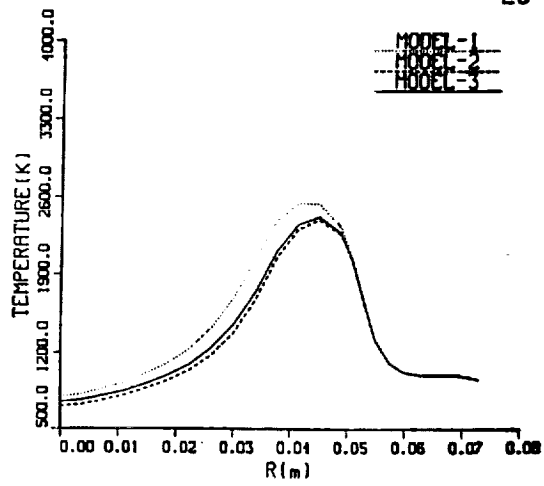

x = 0.04

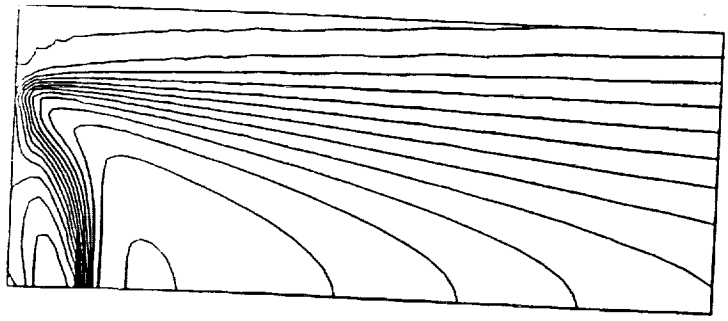

(b) Model II

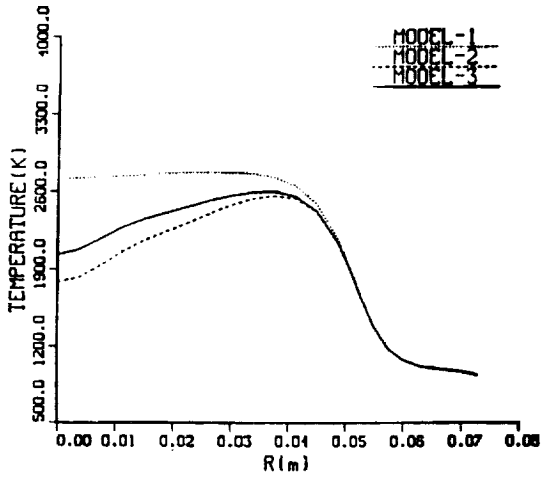

x = 0.08

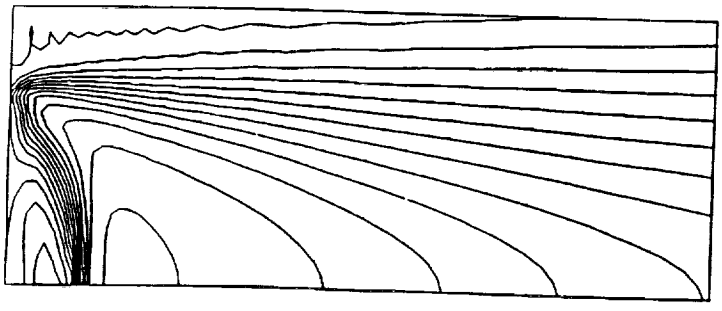

(c) Model III

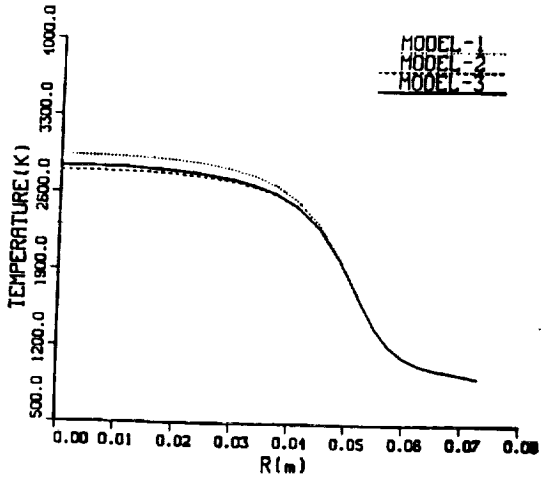

x = 0.12

FIG 6 Contours of Temperature for Three Vaporization Models, Contour Interval 50°K, Minimum 700°K, Maximum 2800°K

FIG 7 Radial Profiles of Temperature for Three Vaporization Models

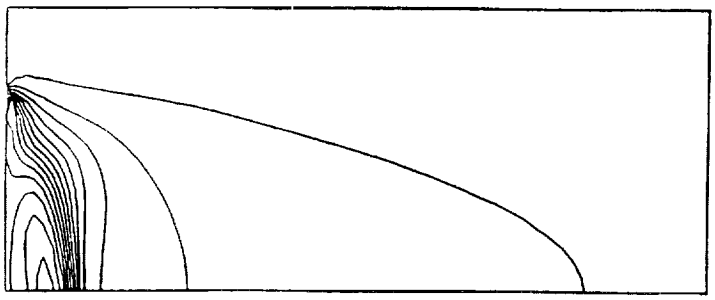

(a) Model I

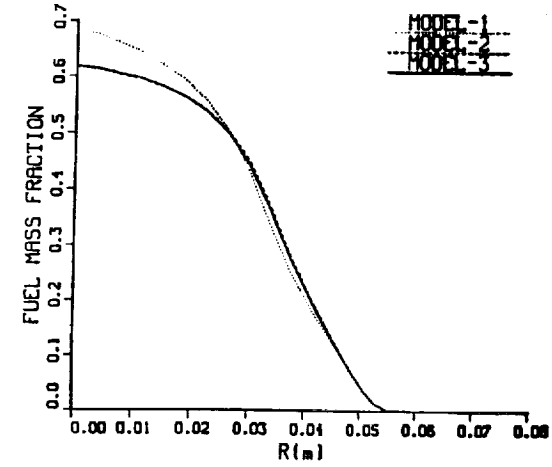

x = 0.04

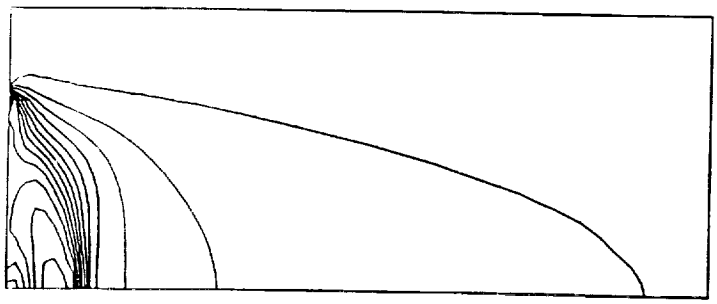

(b) Model II

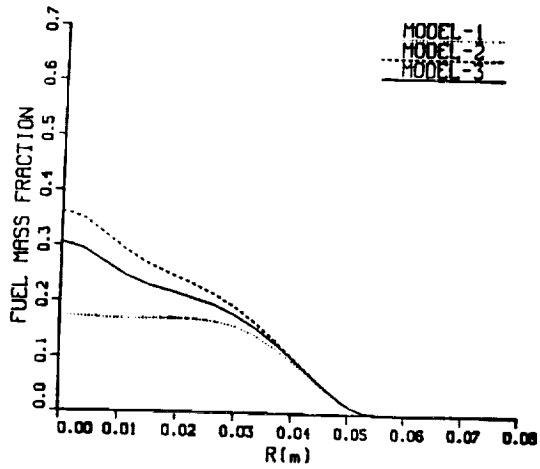

x = 0.08

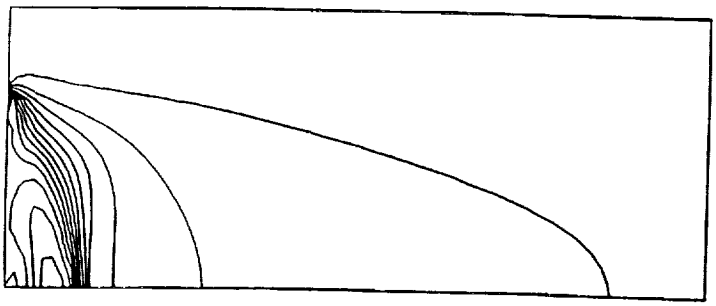

(c) Model III

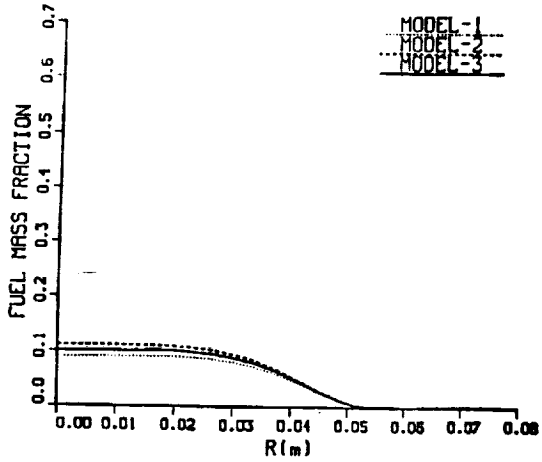

x = 0.12

FIG 8 Fuel Mass Fractions, Contour Interval 0.05, Minimum 0.05, Maximum 0.655

FIG 9 Fuel Mass Fractions in Radial Direction